Chern-Simons orbital magnetoelectric coupling in generic insulators

Sinisa Coh,[1,*] David Vanderbilt,[1] Andrei Malashevich,[2] and Ivo Souza[3]
[1]*Department of Physics Astronomy, Rutgers University, Piscataway, New Jersey 08854-8019, USA*
[2]*Department of Physics, University of California, Berkeley, California 94720, USA*
[3]*Centro de Física de Materiales and DIPC, Universidad del País Vasco, 20018 San Sebastián, Spain and Ikerbasque, Basque Foundation for Science, E-48011 Bilbao, Spain*
(Received 28 October 2010; revised manuscript received 7 January 2011; published 23 February 2011)

We present a Wannier-based method to calculate the Chern-Simons orbital magnetoelectric coupling in the framework of first-principles density-functional theory. In view of recent developments in connection with strong $\mathbb{Z}_2$ topological insulators, we anticipate that the Chern-Simons contribution to the magnetoelectric coupling could, in special cases, be as large or larger than the total magnetoelectric coupling in known magnetoelectrics, such as Cr_2O_3. The results of our calculations for the ordinary magnetoelectrics Cr_2O_3, $BiFeO_3$, and $GdAlO_3$ confirm that the Chern-Simons contribution is quite small in these cases. On the other hand, we show that, if the spatial-inversion and time-reversal symmetries of the $\mathbb{Z}_2$ topological insulator Bi_2Se_3 are broken by hand, large induced changes appear in the Chern-Simons magnetoelectric coupling.

DOI: 10.1103/PhysRevB.83.085108 PACS number(s): 71.15.Rf, 75.85.+t, 03.65.Vf

I. INTRODUCTION

In recent years, there has been a significant revival of interest in magnetoelectric effects in solids, as surveyed in several reviews.[1–4] Potential applications of these materials have long been discussed[5,6] in areas ranging from the optical manipulation and frequency conversion to magnetoelectric memories. Of the various quantities that can be discussed, the linear magnetoelectric coupling tensor α_{ij} is clearly of primary interest, as it quantifies the leading-order term in the coupling at small fields. We define it as

$$\alpha_{ij} = \left(\frac{\partial \mathcal{P}_i}{\partial B_j}\right)_{\mathcal{E}} = \left(\frac{\partial M_j}{\partial \mathcal{E}_i}\right)_{B}, \tag{1}$$

where $\mathcal{P}_i$ is the electric polarization induced by the magnetic field B_j, or equivalently, M_j is the magnetization induced by the electric field $\mathcal{E}_i$. We use SI units (see Sec. II A), and the derivatives are to be evaluated at zero electric and magnetic fields. In the special case that the induced response ($\boldsymbol{\mathcal{P}}$ or $\mathbf{M}$) remains parallel to the applied field ($\mathbf{B}$ or $\boldsymbol{\mathcal{E}}$), the tensor $\boldsymbol{\alpha}$ is purely diagonal with equal diagonal elements, and its strength can be measured by a dimensionless scalar parameter θ defined via

$$\alpha_{ij}^{\mathrm{iso}} = \frac{\theta e^2}{2\pi h}\delta_{ij}. \tag{2}$$

More generally, depending on the magnetic point group of the crystal, α_{ij} can have distinct diagonal components as well as nonzero off-diagonal ones.

The linear magnetoelectric response α_{ij} can be decomposed into two contributions coming from purely electronic and from ionic responses, respectively. The former is defined as the magnetoelectric response that occurs when atoms are not allowed to displace in response to the applied field, while the latter is defined as the remaining lattice-mediated response. One generally expects ionic effects to dominate over electronic responses, as, for example, was shown recently in Refs. 7 and 8 for the case of Cr_2O_3. Moreover, each of these components can be decomposed further into spin and orbital parts, since the magnetization induced by the electric field can be decomposed in that way. Here, one would naively expect that the spin contribution will dominate with respect to the orbital one, since orbital moments are usually strongly quenched by crystal fields. Mostly for this reason, realistic theoretical calculations of magnetoelectric coupling have been developed[7–9] only for the spin component.

As shown in Refs. 10 and 11 using two complementary approaches, the orbital magnetoelectric polarizability (OMP), defined as the contribution of orbital currents to the magnetoelectric coupling α_{ij}, can be written as the sum of three gauge-invariant contributions. One of these, first discussed by Qi *et al.*[12] and Essin *et al.*,[13] is the Chern-Simons orbital magnetoelectric polarizability (CSOMP) term. Since this contribution is purely isotropic, it contributes only to θ, as in Eq. (2). In this paper, we will focus mostly on the CSOMP component of α_{ij}. From an implementation viewpoint, the CSOMP component is quite different from the other two components of the OMP: It can be calculated from knowledge of the ground-state electron wave functions alone but only after careful attention is given to the need to choose a smooth gauge in discretized k space.

One of the motivations for this paper is the possibility of finding a material whose CSOMP component of the linear magnetoelectric tensor will be large compared to the total coupling in known magnetoelectric materials. As elaborated in more detail in Sec. II, the basis for this possibility arises from the before-mentioned theoretical developments[14] and the experimental verification of the existence of $\mathbb{Z}_2$ topological insulators, such as $Bi_{1-x}Sb_x$, Bi_2Se_3, Bi_2Te_3, and Sb_2Te_3.[15–17] Roughly speaking, we seek a material that is similar to a $\mathbb{Z}_2$ topological insulator but having broken inversion and time-reversal symmetries. In order to take the first steps toward searching for such materials, we have set out to calculate the CSOMP component of the magnetoelectric tensor in several compounds of interest using density-functional theory.

This paper is organized as follows. In Sec. II, we provide theoretical background by reviewing the previously derived[10,11] expression for the $\boldsymbol{\alpha}$ tensor and by discussing the connection between bulk and surface properties in a way

that is analogous to the theory of surface charge and bulk electric polarization. We also review the connection to $\mathbb{Z}_2$ topological insulators and make some general comments about symmetry. In Sec. III, we discuss the gauge-fixing issues that arise when discretizing the CSOMP expression on a k-point mesh and show how these can be resolved using Wannier-based methods. By this route, we arrive at an explicit expression for the CSOMP in terms of position matrix elements between Wannier functions (WFs). We evaluate this expression in the density-functional context for several materials of interest in Sec. IV. Finally, we summarize and give an outlook in Sec. V.

II. BACKGROUND AND MOTIVATION

In this section, we briefly summarize previous work from Refs. 10 and 11 on the OMP, describe relationships between bulk and surface properties, discuss motivations for this paper based on the discovery of strong $\mathbb{Z}_2$ topological insulators, and present a brief symmetry analysis.

A. Units and conventions

In this paper, we use SI units and define α according to Eq. (1) using independent field variables $\mathcal{E}$ and B. It follows that α has the same units as the vacuum admittance $1/c\mu_0$.[18] While this is convenient from the point of view of first-principles theory, where B is fixed to zero in practice, the more conventional definition in the literature is in terms of fixed $\mathcal{E}$ and H fields, in which case, one has

$$\alpha_{ij}^{\mathrm{EH}} = \left(\frac{\partial \mathcal{P}_i}{\partial H_j}\right)_{\mathcal{E}} = \mu_0 \left(\frac{\partial M_j}{\partial \mathcal{E}_i}\right)_{H}, \tag{3}$$

and α^{EH} has units of inverse velocity.[19] In the typical case that the magnetic susceptibility of the material is negligible, these are related by $\alpha^{\mathrm{EH}} = \alpha\mu_0$, and one can define a reduced (dimensionless) quantity $\alpha_{\mathrm{r}} = c\mu_0\alpha = c\alpha^{\mathrm{EH}}$.[18] Defined in this way, α_{r} is numerically equal to the value of the magnetoelectric coupling in Gaussian units using the conventions of Rivera,[19] which, in turn, corresponds to the notation g.u. (Gaussian units) in some recent papers.[7,9] Furthermore, using the notation of Eq. (2) for the isotropic magnetoelectric coupling, it follows that the diagonal component of α_{r} is just θ/π times the fine structure constant (which is $e^2c\mu_0/2h$ in SI units).

B. Theory of orbital magnetoelectric coupling

The purely electronic orbital magnetoelectric coupling α_{ij} can be written in terms of three gauge-invariant contributions,

$$\alpha_{ij} = \alpha_{ij}^{\mathrm{CS}} + \widetilde{\alpha}_{ij}^{\mathrm{LC}} + \widetilde{\alpha}_{ij}^{\mathrm{IC}}, \tag{4}$$

where $\alpha_{ij}^{\mathrm{CS}} = \delta_{ij}\alpha^{\mathrm{CS}}$ is the above-mentioned (isotropic) CSOMP, while $\widetilde{\alpha}_{ij}^{\mathrm{LC}}$ and $\widetilde{\alpha}_{ij}^{\mathrm{IC}}$ are two additional contributions. The isotropic part of the OMP tensor has contributions from the two $\widetilde{\alpha}$ terms as well as from the CSOMP term. The three contributions to the OMP can compactly be expressed as

$$\alpha^{\mathrm{CS}} = \eta\frac{e}{2}\int d^3k\,\epsilon_{ijk}\,\mathrm{tr}\left[\mathcal{A}_i\,\partial_j\mathcal{A}_k - \frac{2i}{3}\mathcal{A}_i\mathcal{A}_j\mathcal{A}_k\right], \tag{5}$$

$$\widetilde{\alpha}_{ij}^{\mathrm{LC}} = \eta\epsilon_{jkl}\,\mathrm{Im}\int d^3k\,\langle\widetilde{\partial}_k u_{n\mathbf{k}}|(\partial_l H_{\mathbf{k}})|\widetilde{D}_i u_{n\mathbf{k}}\rangle, \tag{6}$$

$$\widetilde{\alpha}_{ij}^{\mathrm{IC}} = \eta\epsilon_{jkl}\,\mathrm{Im}\int d^3k\,\langle\widetilde{\partial}_k u_{n\mathbf{k}}|\widetilde{D}_i u_{m\mathbf{k}}\rangle\langle u_{m\mathbf{k}}|(\partial_l H_{\mathbf{k}})|u_{n\mathbf{k}}\rangle, \tag{7}$$

where the notations are defined as follows. An implied sum notation applies to repeated Cartesian $(ijkl)$ and band (mn) indices, corresponding to a trace over occupied bands in the latter case (written explicitly as tr). A common prefactor $\eta = -e/\hbar(2\pi)^3$ appears in each equation, with $e > 0$ being the magnitude of the electron charge. The Berry connection,

$$\mathcal{A}_{mn\mathbf{k}j} = \langle u_{m\mathbf{k}}|i\,\partial_j|u_{n\mathbf{k}}\rangle \tag{8}$$

is defined in terms of the cell-periodic Bloch functions,

$$|u_{n\mathbf{k}}\rangle = e^{-i\mathbf{k}\cdot\mathbf{r}}|\psi_{n\mathbf{k}}\rangle, \tag{9}$$

which are the eigenvectors of $H_{\mathbf{k}} = e^{-i\mathbf{k}\cdot\mathbf{r}}\mathcal{H}e^{i\mathbf{k}\cdot\mathbf{r}}$, where $\mathcal{H}$ is the bulk periodic Hamiltonian of the crystal at zero electric and magnetic fields. ∂_j and D_j are the partial derivatives with respect to the jth component of the wave vector $\mathbf{k}$ and the electric field $\boldsymbol{\mathcal{E}}$, respectively. Finally, the tilde indicates a covariant derivative, $\widetilde{\partial}_j = Q_{\mathbf{k}}\partial_j$ and $\widetilde{D}_j = Q_{\mathbf{k}}D_j$, where $Q_{\mathbf{k}} = 1 - |u_{n\mathbf{k}}\rangle\langle u_{n\mathbf{k}}|$ (sum implied over n). Additional screening contributions to $\widetilde{\alpha}_{ij}^{\mathrm{LC}}$ and $\widetilde{\alpha}_{ij}^{\mathrm{IC}}$ that occur in the context of self-consistent field calculations, not given here, can be found in Ref. 11.

As in the case of electronic polarization, one needs to be careful about relating the above bulk expressions to experimentally measurable physical quantities, since arbitrary surface modifications can contribute to the effective measurable OMP. The relationship between the OMP and the experimentally measurable responses are explained in more detail in Sec. II C.

C. Relation between bulk and surface properties

In order to discuss the relationship between bulk and surface quantities in connection with the OMP, it is instructive first to review the corresponding connections in the theory of electric polarization.

1. Electric polarization and surface charge

We first review the relationship between the bulk electric polarization, as obtained from the crystal band structure according to the Berry-phase theory,[20,21] and a measurable quantity, which is the macroscopic dipole moment of a finite sample cut from this crystal. Given the set of valence Bloch wave functions $|\psi_{n\mathbf{k}}\rangle$ of an insulating crystal, one can readily calculate the electronic contribution to the polarization as the integral,

$$\mathcal{P}_i = -\frac{e}{(2\pi)^3}\sum_n\int d^3k\,\langle u_{n\mathbf{k}}|i\,\partial_{k_i}|u_{n\mathbf{k}}\rangle, \tag{10}$$

over the Brillouin zone (BZ). Gauge changes ($|u_{n\mathbf{k}}\rangle \to e^{-i\beta(\mathbf{k})}|u_{n\mathbf{k}}\rangle$) can change the value of this integral only by $\mathbf{R}e/\Omega$, where $\mathbf{R}$ is a lattice vector and Ω is the unit cell volume. Therefore, the value of this integral is only well-defined mod $\mathbf{R}e/\Omega$. In what follows, we assume that a definite choice of gauge has been made so that a definite value of $\mathcal{P}$ has been established. We now analyze how, and under what circumstances, one can relate this $\mathcal{P}$ to the (experimentally measurable) dipole moment $\mathbf{d}$ of an arbitrarily faceted finite sample of this crystal.

At each local region on the surface of this finite sample, assuming a perfect surface preparation (defect free with ideal periodicity), we can relate $\mathcal{P}$ to the surface charge density σ at that same point via[21]

$$\sigma = \left(\mathcal{P} + \frac{e}{\Omega}\mathbf{R}\right)\cdot\hat{n} + \Delta. \tag{11}$$

Here, $\hat{n}$ is the surface normal unit vector, $\mathbf{R}$ is a lattice vector, and Δ is an additional contribution present only for metallic surfaces. The term involving $\mathbf{R}$, which corresponds to an integer number of electrons per surface unit cell, is required because, for a given surface $\hat{n}$, it may be possible to prepare the surface in different ways (e.g., by adding or subtracting a layer of ions, or by filling or emptying a surface band) such that the surface charge per cell changes by a quantum. Thus, $\mathbf{R}$ is, in general, a surface-dependent quantity in Eq. (11). If the surface patch under consideration is not insulating, then Δ is a term that measures the contribution of the partially occupied surface bands to the surface charge and is proportional to the area fraction of occupied band in k space. (In the case of an insulator with a nonzero first Chern number, this fraction has to be calculated with special care,[22] but we will not consider this case in what follows.)

Now, let us consider the special case that all surfaces are insulating ($\Delta = 0$) and that the surface charges of *all* surface patches are consistent with a *single* vector value of $\mathbf{R}$ (global consistency). Under these circumstances, the macroscopic dipole moment $\mathbf{d}$ of the crystallite is given by

$$\mathbf{d} = \mathcal{V}\left(\mathcal{P} + \frac{e}{\Omega}\mathbf{R}\right), \tag{12}$$

which can be obtained trivially by integrating Eq. (11). Here, $\mathcal{V}$ is the volume of the entire finite sample. As could be anticipated, $\mathbf{d}/\mathcal{V}$ has a component depending only on the bulk wave functions and our gauge choice and an additional component $e\mathbf{R}/\Omega$ reflecting the preparation of the surfaces.

2. OMP and surface anomalous Hall conductivity

We now discuss a corresponding set of relationships between the bulk-calculated OMP and the surface anomalous Hall conductivity.

Using Eqs. (5)–(7), one can calculate the tensor $\boldsymbol{\alpha}$ from the knowledge of the bulk Hamiltonian of an insulating crystal. Analogously, as in the case of polarization, one can again show that a gauge change[23] must either leave $\boldsymbol{\alpha}$ invariant or change it by a quantum $m(e^2/h)\mathbf{I}$, where m is an integer and $\mathbf{I}$ is the unit matrix. More precisely, this gauge transformation will only affect the CSOMP component $\boldsymbol{\alpha}^{\mathrm{CS}}$ of the OMP, since the other two contributions $\tilde{\boldsymbol{\alpha}}^{\mathrm{LC}}$ and $\tilde{\boldsymbol{\alpha}}^{\mathrm{IC}}$ are fully gauge invariant (see Ref. 11 for details).

We now imagine cutting a finite crystallite from this infinite crystal, and we wish to relate $\boldsymbol{\alpha}$ to its physically observable linear magnetoelectric coupling $\boldsymbol{\beta}$, defined for a finite sample by

$$\beta_{ij} = \frac{\partial d_i}{\partial B_j} = \frac{\partial \mu_j}{\partial \mathcal{E}_i}, \tag{13}$$

where d_i is the dipole moment of the finite sample and μ_j is its magnetic dipole moment. We want to discuss this relationship in a way that is analogous to that between the bulk $\mathcal{P}$ and the sample dipole moment $\mathbf{d}$ in Sec. II C 1.

As follows from Eq. (1), the application of an electric field $\mathcal{E}_j$ to the insulating crystal induces the magnetization,

$$M_k = \alpha_{jk}\mathcal{E}_j, \tag{14}$$

where $\boldsymbol{\alpha}$ is given by Eq. (4) and is only determined mod $m(e^2/h)\mathbf{I}$. Having a homogeneous M_k inside the sample and $M_k = 0$ outside is equivalent to having a surface current K_i equal to

$$K_i = \epsilon_{ikl}M_k n_l, \tag{15}$$

where n_l is the surface unit normal. By eliminating M_k from these equations, we see that having a magnetoelectric tensor $\boldsymbol{\alpha}$ is equivalent to having a surface anomalous Hall conductivity $\sigma_{ij}^{\mathrm{AH}} = \epsilon_{ikl}\alpha_{jk}n_l$. If the surface patch in question is insulating, then its anomalous Hall conductivity should just be given by this equation. If, instead, the surface patch is metallic, then an additional surface contribution Δ_{ij} should be present, leading to the relation

$$\sigma_{ij}^{\mathrm{AH}} = \epsilon_{ikl}\left(\alpha_{jk} + m\frac{e^2}{h}\delta_{jk}\right)n_l + \Delta_{ij}. \tag{16}$$

This equation is in precise analogy to Eq. (11) relating the polarization to the surface charge. Here, Δ_{ij} may, in general, contain dissipative contributions, but in the dirty limit, it will be dominated by the intrinsic surface contribution that can be calculated as a two-dimensional (2D) BZ integral of the Berry curvature of the occupied surface states.[24] The integer quantum m appearing in Eq. (16) corresponds to the theoretical possibility that the surface preparation can be changed in such a way that a surface band having a nonzero Chern number may become occupied. For example, this could be done, in principle, by constructing a 2D quantum anomalous Hall layer (as described, e.g., by the Haldane model[25]), straining it to be commensurate with the surface, and adiabatically turning on hopping matrix elements to stitch it onto the surface.

In the special case that all surface patches are insulating ($\Delta_{ij} = 0$), and all surface patches have an anomalous Hall conductivity given by Eq. (16) with the *same* value of m (global consistency), we can relate the experimentally measurable magnetoelectric response $\boldsymbol{\beta}$ of the finite crystallite to the bulk-calculated $\boldsymbol{\alpha}$ via

$$\boldsymbol{\beta} = \mathcal{V}\left(\boldsymbol{\alpha} + m\frac{e^2}{h}\mathbf{I}\right), \tag{17}$$

which follows by integrating Eq. (16) over all surfaces. This equation is in close analogy to Eq. (12) for the case of electric polarization. In particular, we see that $\boldsymbol{\beta}/\mathcal{V}$ has a component $\boldsymbol{\alpha}$ depending only on the bulk wave functions and our gauge choice and an additional component that is an integer multiple of $(e^2/h)\mathbf{I}$, reflecting the preparation of the surfaces.

As will be discussed in Sec. II D, time-reversal symmetry imposes additional constraints on $\boldsymbol{\alpha}$, and some care is needed in the interpretation of Eq. (17) for the case of $\mathbb{Z}_2$ topological insulators.

D. Motivation and relationship to strong $\mathbb{Z}_2$ topological insulators

In this section, we give arguments to motivate our hope that, in certain materials, the CSOMP might be on the order of, or even much larger than, the total magnetoelectric coupling in typical known magnetoelectric materials. For simplicity, henceforth, we focus only on the CSOMP part of the total OMP response, although there are additional contributions coming from $\widetilde{\alpha}^{\mathrm{LC}}$ and $\widetilde{\alpha}^{\mathrm{IC}}$. Thus, from now on, the quantity θ measures the strength of the CSOMP through the relation $\alpha^{\mathrm{CS}} = \theta e^2/2\pi h$.

1. Time-reversal symmetry constraints on θ

Let us analyze the allowed values of θ for an infinite bulk insulating system that respects time-reversal (T) symmetry. Since T flips the sign of the magnetic field, it will also reverse the sign of θ. As mentioned earlier in Sec. II C 2, however, the value of θ can be changed by 2π under a gauge transformation. Therefore, one concludes[12,13] that the allowed values of θ consistent with T symmetry are 0 and π (each mod 2π) and that these two cases provide a topological classification of all T-invariant insulators. Indeed, this classification has been shown[12,13] to be identical to the one based on the $\mathbb{Z}_2$ index, with $\mathbb{Z}_2$-odd or strong topological insulators having $\theta = \pi$, while $\mathbb{Z}_2$-even or normal insulators have $\theta = 0$, although the $\mathbb{Z}_2$ index is most often introduced in a different context.[26] (Incidentally, $\widetilde{\boldsymbol{\alpha}}^{\mathrm{LC}} = \widetilde{\boldsymbol{\alpha}}^{\mathrm{IC}} = 0$ in both cases since these terms are fully gauge independent, unlike the CSOMP term, which can be changed by 2π.)

Consider now a finite sample of a normal ($\mathbb{Z}_2$-even) T-symmetric insulator ($\theta = 0$ in the bulk) with insulating surfaces ($\Delta_{ij} = 0$) prepared in a way that the integer m is nonzero and the same on every surface. From Eq. (17), we conclude that this sample will have a nonzero magnetoelectric response $\boldsymbol{\beta}$, proportional to m. Obviously, a sample that has T symmetry both in the bulk and on the surface must have $\boldsymbol{\beta} = 0$, and, therefore, we conclude that this system needs to have broken T-reversal symmetry at the surface. As mentioned earlier, one could, at least formally, prepare such a surface by starting from the one that has $m = 0$ and then absorbing, to each surface, a layer of anomalous Hall insulator[25] with Chern index m. Such a procedure will keep the surfaces insulating, but it will necessarily break the T-reversal symmetry.

Next, we analyze the case of a strong $\mathbb{Z}_2$ topological insulator having $\theta = \pi$, or equivalently, $\boldsymbol{\alpha} = \boldsymbol{\alpha}^{\mathrm{CS}} = (e^2/2h)\,\mathbf{I}$. We first consider a sample of such a system that has T symmetry conserved at its surfaces, as in Fig. 1(a). Again, since the entire sample is T symmetric, its experimentally measurable magnetoelectric coupling tensor $\boldsymbol{\beta}$ clearly has to vanish. Using Eq. (16) and the fact that m can take on only integer, and not half-integer, values, we conclude that the only way to make the response of the entire sample vanish is to have Δ_{ij} be nonzero. This requires that the surfaces of such a system must be metallic. Moreover, since the contribution Δ_{ij} of the metallic surface band to the surface anomalous Hall conductivity is just given by the Berry phase around the Fermi loop,[24] the needed cancellation requires this Berry phase to be exactly $\pm\pi$. All this is in precise accord with the known properties of $\mathbb{Z}_2$-odd insulators and their topologically protected surface states.[26]

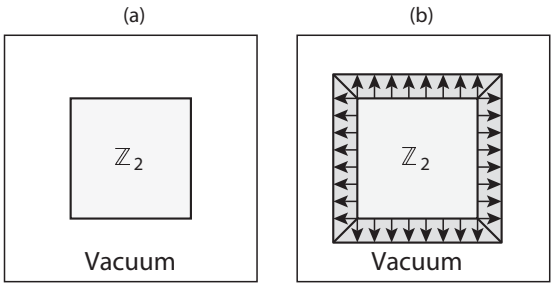

FIG. 1. Identical samples cut from a strong $\mathbb{Z}_2$ topological insulator but with two different surface preparations. (a) Time-reversal symmetry is preserved at vacuum-terminated surfaces; the net magnetoelectric coupling of this sample is zero. (b) Time-reversal symmetry is broken at the surface as a result of exchange coupling to an insulating ferromagnetic adlayer; if this opens a gap in the surface-state spectrum, the entire sample will behave as if it has a magnetoelectric coupling of exactly $\theta = \pi$.

The Kramers degeneracy at the Dirac cone in the surface band structure can be removed by the application of a T-breaking perturbation to the surface. In principle, this could be accomplished, for example, by applying a local magnetic field to the surface or by interfacing the surface to an insulating magnetic overlayer. In the latter case, the interatomic exchange couplings provide a kind of effective magnetic field acting on the surface layer of the topological insulator. If the local Fermi level resides in the gap opened by field, then the surface becomes insulating. If the field can be consistently oriented (see Ref. 12) on each patch of the surface, either along or opposite the direction of surface normal vector $\mathbf{n}$ [as shown in Fig. 1(b)], then the entire surface becomes insulating. It is important that the field is applied consistently in the same direction with respect to $\mathbf{n}$, since conducting channels will otherwise appear at domain boundaries.[26]

If all of these requirements are met, the surface contribution Δ_{ij} to $\boldsymbol{\beta}$ vanishes so that $\boldsymbol{\beta} = \mathcal{V}\boldsymbol{\alpha}$ with $\boldsymbol{\alpha}$ given only by bulk value of $\theta = \pi$ (assuming $m = 0$ for simplicity). Therefore, such a sample of a strong $\mathbb{Z}_2$ topological insulator would behave as if the entire sample has exactly half a quantum of magnetoelectric coupling ($\theta = \pi$), although its bulk is time-reversal symmetric!

2. Prospects for large-θ materials

Recently, surface-sensitive angle-resolved photoemission spectroscopy measurements have experimentally confirmed that several compounds,[15–17] including $Bi_{1-x}Sb_x$, Bi_2Se_3, Bi_2Te_3, and Sb_2Te_3, do indeed behave as strong $\mathbb{Z}_2$ topological insulators. Therefore, their bulk wave functions must be characterized by $\theta = \pi$. Until now, the corresponding magnetoelectric response has not been measured experimentally, in part because of the difficulties in obtaining truly insulating behavior in the bulk, as well as the need to gap the surfaces by putting them in contact with magnetic overlayers as described earlier.

We believe that a more promising approach to observing a large CSOMP (i.e., θ comparable to π) is to consider an insulator that has neither T nor spatial-inversion symmetry. In this

case, the $\mathbb{Z}_2$ classification does not apply, and the surface can be gapped without any need to apply a T-breaking perturbation. (A more precise statement of the symmetry considerations will be given in Sec. II E.) Then, the sample can display a bulk magnetoelectric coupling of the simple form $\boldsymbol{\beta} = \mathcal{V}\boldsymbol{\alpha}$. We note that an orbital magnetoelectric coupling of $\theta \simeq \pi$ (i.e., $\alpha_r \simeq 1/137$) would correspond to $\alpha^{\mathrm{EH}} \simeq 24.3$ ps/m, a value that is significantly larger than the observed coupling in Cr_2O_3, one of the best-studied magnetoelectric materials. For comparison, the reported experimental values for $\alpha_\perp^{\mathrm{EH}}$ in Cr_2O_3, which are presumably dominated by spin-lattice coupling, range between 0.7 and 1.6 ps/m at 4.2 K.[27,28]

Of course, in order to have a good chance of finding a material with a large θ, it may be advisable to look for materials with some of the same characteristics as the known $\mathbb{Z}_2$-odd insulators, of which the most important is probably the presence of heavy atoms with strong spin-orbit coupling. We see no strong reason why such a search might not reveal a material having a large OMP in the above sense.

To illustrate the kind of a search we have in mind, consider some model Hamiltonian that depends on two parameters, one that preserves either the T or spatial-inversion symmetry (or both), and another that that breaks symmetry such that θ takes a generic value. The possible behavior of such a model is sketched in Fig. 2, where these two parameters are plotted along the horizontal and vertical axes, respectively. The figure also indicates the generic value of θ in each region of parameter space. Along the horizontal axis, where the extra symmetry is present, three regions are indicated. The black dot indicates a point of gap closure forming the boundary between a normal T-symmetric insulator regime on the left ($\theta = 0$) and a strong $\mathbb{Z}_2$ topological insulator regime on the right ($\theta = \pi$). If the system is carried along the horizontal axis, θ must be either 0 or π except at the critical point, and, therefore, it must jump discontinuously when passing through this point of metallic behavior. On the other hand, if we now imagine passing from the $\mathbb{Z}_2$-odd to the $\mathbb{Z}_2$-even phase along the dashed curve in Fig. 2, θ can vary smoothly and continuously from π to 0 without any gap closure anywhere along the path. If we can identify a material lying near, but not at, the right end of this dashed path, it could be the kind of large-θ material we seek.

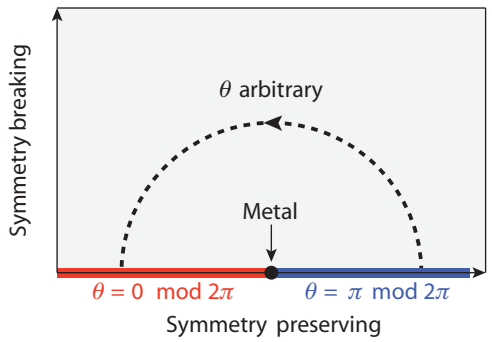

FIG. 2. (Color online) Schematic of the allowable values of θ in different parts of the two-parameter space of some unspecified model Hamiltonian. Horizontal axis corresponds to the perturbation that preserves at least one of the symmetries that renders θ to be 0 or π (see Sec. II E). Vertical axis parametrizes a perturbation that breaks those symmetries and allows θ to be arbitrary. See text for the details.

TABLE I. Magnetic point groups for which a generic nonzero CSOMP is allowed by symmetry. Notation follows Ref. 29. Point groups in bold allow only for a purely isotropic magnetoelectric tensor.

1	$\bar{1}'$	2	m'	$2/m'$	222	$m'm'2$
$m'm'm'$	4	$\bar{4}'$	$4/m'$	3	$\bar{3}'$	6
$\bar{6}'$	$6/m'$	422	$4m'm'$	$\bar{4}'2m'$	$4/m'm'm'$	32
$3m'$	$\bar{3}'m'$	622	$6m'm'$	$\bar{6}'m'2$	$6/m'm'm'$	
23	**m′3**	**432**	**$\bar{4}'$3m′**	**m′3m′**		

Thus, our ultimate goal is to use first-principles calculations to search for a large θ, not in a topological insulator, but in an ordinary (but presumably strongly spin-orbit coupled) insulating magnetic material. While our work has yet to result in the identification of a large-θ material of this kind, it represents the first step in the desired direction.

E. General symmetry considerations

Recall that θ is a pseudoscalar that changes sign under time-reversal and spatial-inversion symmetries (since $\mathbf{B}$ changes sign under T while $\boldsymbol{\mathcal{E}}$ changes sign under inversion). On the other hand, θ is invariant under any translation or proper rotation of a crystal. Therefore, if the magnetic point group of a crystal contains an element that involves T, possibly combined with a proper rotation, the value of θ is constrained to be 0 or π (mod 2π) as discussed earlier. The same happens if the magnetic point group contains inversion symmetry or any other improper rotation.

All 32 of the 122 magnetic point groups that do not contain such symmetry elements, and which, therefore, allow for an arbitrary value of θ, are listed in Table I. (The bold entries in the table are those magnetic groups for which the tensor $\boldsymbol{\alpha}$ must be isotropic, i.e., a constant times the identity matrix; the same magnetic groups were also analyzed in Ref. 18.) Clearly, we can constrain our search for interesting materials to the cases listed in the table.

III. METHODS

In this section, we present our methods for calculating the CSOMP in the framework of density-functional theory and analyze, in more detail, its mathematical properties and the formal similarities to the formulas used to calculate electric polarization and anomalous Hall conductivity.

A. Review of Berry formalism

Assume we are given the Bloch wave functions $|\psi_{n\mathbf{k}}\rangle = e^{i\mathbf{k}\cdot\mathbf{r}}|u_{n\mathbf{k}}\rangle$ as a function of wave vector $\mathbf{k}$ in the d-dimensional BZ ($d = 1$, 2, or 3) for an insulator having valence bands indexed by $n \in \{1, \ldots, N\}$. We work with the cell-periodic Bloch functions $u_{n\mathbf{k}}(\mathbf{r}) = e^{-i\mathbf{k}\cdot\mathbf{r}}\psi_{n\mathbf{k}}(\mathbf{r})$ and allow them to be mixed at each k point by an arbitrary k-dependent unitary matrix

$$|u_{n\mathbf{k}}\rangle \to |u_{m\mathbf{k}}\rangle U_{mn\mathbf{k}} \tag{18}$$

(sum on m implied). After this gauge transformation, the wave functions are no longer eigenfunctions of the Hamiltonian, but they span the same N-dimensional subset of the Hilbert space

as the true eigenfunctions. For any given choice of gauge, we define the Berry connection,

$$\mathcal{A}_{mn\mathbf{k}j} = \langle u_{m\mathbf{k}} | i \frac{\partial}{\partial k_j} | u_{n\mathbf{k}} \rangle, \tag{19}$$

which is a k-dependent $N \times N \times d$ matrix that measures, at each k point, the infinitesimal phase difference between the mth and the nth wave functions associated with neighboring points along Cartesian direction j in k space. This object already was introduced briefly in Eq. (8).

In the context of electronic structure calculations, we can now list three material properties that can be evaluated knowing only the Berry connection: the electric polarization, the intrinsic anomalous Hall conductivity, and the CSOMP.

The electric polarization $\mathcal{P}$ already appears in dimension $d = 1$, and it can be evaluated as an integral of the Berry connection over the one-dimensional BZ as[20]

$$\mathcal{P} = -\frac{e}{2\pi} \int_{\mathrm{BZ}} dk \, \mathrm{tr} \, \mathcal{A}_k, \tag{20}$$

where the trace is performed over the band indices of the Berry connection, as in Eq. (10). The integrand is also referred to as the Chern-Simons 1-form, and its integral over the BZ is well known to be defined only modulo 2π. Any periodic adiabatic evolution of the Hamiltonian $\mathcal{H}(\lambda)$ whose first Chern number in (k,λ) space is nonzero will change the integral above by a multiple of 2π.[20]

Unlike one-dimensional systems, crystals in $d = 2$ can have an anomalous Hall conductivity. For a metal, the intrinsic contribution from a band crossing the Fermi level can be evaluated as a line integral,[24,30]

$$\sigma^{\mathrm{AH}} = \frac{e^2}{h} \frac{1}{2\pi} \oint_{\mathrm{FL}} d\mathbf{k} \cdot \boldsymbol{\mathcal{A}}_{\mathbf{k}}, \tag{21}$$

over the Fermi loop. Fully filled deeper bands can also make a quantized contribution given by a similar integral but around the entire BZ; this is the only contribution in the case of a quantum anomalous Hall insulator.[25] (In both cases, the gauge choice on the boundary of the region should be consistent with a continuous, but not necessarily k-periodic, gauge in its interior; alternatively, each expression can be converted to an area integral of a Berry curvature to resolve any uncertainty about branch choice. See Ref. 31 for more details.)

Finally, unlike one- or two-dimensional systems, three-dimensional systems can have an isotropic magnetoelectric coupling. The CSOMP can be evaluated in $d = 3$ as a BZ integration of a quantity involving the Berry connection:

$$\theta = -\frac{1}{4\pi} \int_{\mathrm{BZ}} d^3k \, \epsilon_{ijk} \, \mathrm{tr} \left[\mathcal{A}_i \partial_j \mathcal{A}_k - \frac{2i}{3} \mathcal{A}_i \mathcal{A}_j \mathcal{A}_k \right]. \tag{22}$$

The integrand in this expression is known as the Chern-Simons 3-form, and its integral over the entire BZ is again ill-defined modulo 2π, since any periodic adiabatic evolution of the Hamiltonian $\mathcal{H}(\lambda)$ whose second Chern number in $(\mathbf{k},\lambda)$ space is nonzero will change θ by an integer multiple of 2π.[12,13]

The sketches in Fig. 3 compare the geometrical characters of the operations needed to evaluate Eqs. (20)–(22) in practice. We consider the case of one occupied electron band for simplicity. The polarization of Eq. (20) is calculated by a line integral; on a discrete k mesh, the integral of the Berry connection $\mathcal{A}$ over each line segment, as in Fig. 3(a), is converted to a discretized form [see Eq. (23)]. Similarly, in two dimensions, the anomalous Hall conductivity of Eq. (21) can be calculated as suggested in Fig. 3(b) by dividing the occupied part of the BZ into small square segments and then by integrating $\mathcal{A}$ around each square. (Equivalently, one can integrate $\mathcal{A}$ along the Fermi loop.[31]) In three dimensions, Fig. 3(c), Eq. (22) can be evaluated by dividing the BZ into small cubes. In each, one needs to multiply the integral of $\mathcal{A}$ along one of the Cartesian directions [as in Eq. (20)] with the integral of the Berry connection in the square orthogonal to that direction [as in Eq. (21)], followed by a symmetrization over the three Cartesian directions.

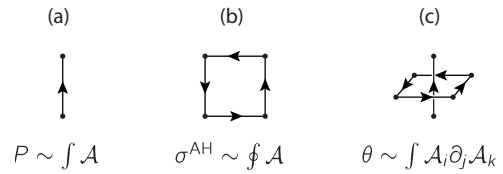

FIG. 3. Graphical interpretation of Eqs. (20) (a), (21) (b), and (22) (c) in the case of one occupied electron band and for cubic crystal symmetry, for simplicity. See text for more details.

B. Numerical evaluation of θ

In electronic-structure calculations, the cell-periodic wave functions $|u_{n\mathbf{k}}\rangle$ are typically calculated on a uniform k-space grid with no special gauge choice; in general, one should assume that the phases have been randomly assigned. Nevertheless, it is straightforward to construct a gauge-invariant polarization formula that is immune to this kind of scrambling of the gauge.[32] In one dimension with k_j for $j \in \{1, \ldots, M\}$ (where k_M is the periodic image of point k_1), the electronic polarization is calculated as

$$P = \frac{e}{2\pi} \, \mathrm{Im} \, \ln \det \left[M_{k_1 k_2} M_{k_2 k_3} \cdots M_{k_{M-1} k_M} \right], \tag{23}$$

where the overlap matrix $M_{kk'}$ is defined as

$$[M_{kk'}]_{mn} = \langle u_{mk} | u_{nk'} \rangle. \tag{24}$$

The reason for using Eq. (23) is that the determinant of the matrix $M_{k_1 k_2} M_{k_2 k_3} \cdots M_{k_{M-1} k_M}$ is gauge invariant under any transformation in the form of Eq. (18). Additionally, the implementation of Eq. (23) is numerically stable even when there are band crossings. A similar gauge-invariant discretization can also be used to calculate the anomalous Hall conductivity σ^{AH}.[31]

Unfortunately, except in the single-band (Abelian) case, we are unaware of any corresponding gauge-invariant discretized formula for the integral of the Chern-Simons 3-form. As a result, we have no prescription for computing the CSOMP that is exactly gauge invariant for a given choice of k mesh. This is a serious problem. Unlike the calculation of the polarization, which is straightforward even if the gauge is randomly scrambled at each mesh point, the calculation of the CSOMP requires that we first identify a reasonably smooth gauge on the discrete mesh.

The problem of finding a smooth gauge in $\mathbf{k}$ is essentially the same as that of finding well-localized WFs. For this reason, here, we have adopted the approach of first constructing a Wannier representation for the valence bands and then using it to compute the CSOMP. In fact, starting from Eq. (22), we derive an expression that allows us to compute θ directly in the Wannier representation. Once we have well-localized WFs, this guarantees smoothness of the gauge and avoids problems with band crossings. Admittedly, such a formula still depends on the gauge choice, meaning that different choices of WFs will lead to slightly different results. However, this difference will vanish as one increases the density of the k-point mesh, since in the continuum limit, the k-space expression for θ is gauge invariant (mod 2π). More precisely, we expect the calculation of θ to converge once the inverse of the k-point mesh spacing becomes much larger than the spread of the WFs.

Therefore, we adopt the strategy of calculating θ on k meshes of different density and extrapolating θ to the limit of an infinitely dense mesh. Furthermore, we construct maximally localized Wannier functions (MLWFs) following Ref. 32, expecting this to give relatively rapid convergence as a function of the k-mesh density.

Recall that the WF associated with (generalized) band index n in unit cell $\mathbf{R}$ is defined in terms of the rotated Bloch states (18) as

$$|\mathbf{R}n\rangle = \frac{\Omega}{(2\pi)^3}\int d^3k\, e^{i\mathbf{k}\cdot(\mathbf{r}-\mathbf{R})}|u_{m\mathbf{k}}\rangle U_{mn\mathbf{k}}. \tag{25}$$

In the case of MLWFs, the $U_{mn\mathbf{k}}$ are chosen in such a way that the total quadratic spread of the WF is minimized.[32] (In practice, the BZ integral is replaced by a summation over a uniform grid of k points.)

Using Eq. (25), one can relate the Berry-connection matrix $\mathcal{A}_{mn\mathbf{k}j}$ in the smooth gauge to the Wannier matrix elements of the position operator through[32]

$$A_{mn\mathbf{k}j} = \sum_{\mathbf{R}} e^{i\mathbf{k}\cdot\mathbf{R}}\langle\mathbf{0}m|r_j|\mathbf{R}n\rangle. \tag{26}$$

Replacing each occurrence of A_j in Eq. (22) with the above gives, after some algebra,

$$\theta = \frac{1}{4\pi}\frac{(2\pi)^3}{\Omega}\epsilon_{ijk}\,\mathrm{Im}\left(\frac{1}{3}\sum_{\mathbf{R}}\langle\mathbf{0}m|r_i|\mathbf{R}n\rangle\langle\mathbf{R}n|r_j|\mathbf{0}m\rangle R_k - \frac{2}{3}\sum_{\mathbf{RP}}\langle\mathbf{0}l|r_i|\mathbf{R}m\rangle\langle\mathbf{R}m|r_j|\mathbf{P}n\rangle\langle\mathbf{P}n|r_k|\mathbf{0}l\rangle\right), \tag{27}$$

where the sum is implied over band (lmn) and Cartesian (ijk) indices. [Although Eqs. (22) and (27) are equivalent as a whole, they do not match term by term.]

To obtain a more symmetric form, we introduce a modified position-operator matrix element between WFs defined as

$$\langle\mathbf{R}m|\tilde{r}_i|\mathbf{P}n\rangle = \langle\mathbf{R}m|r_i|\mathbf{P}n\rangle(1-\delta_{mn}\delta_{\mathbf{RP}}), \tag{28}$$

and a notation for the Wannier center,

$$\tau_{ni} = \langle\mathbf{0}n|r_i|\mathbf{0}n\rangle. \tag{29}$$

Then, Eq. (27) becomes

$$\theta = \frac{1}{4\pi}\frac{(2\pi)^3}{\Omega}\epsilon_{ijk} \times \mathrm{Im}\left[\sum_{\mathbf{R}}\langle\mathbf{0}m|\tilde{r}_i|\mathbf{R}n\rangle\langle\mathbf{R}n|\tilde{r}_j|\mathbf{0}m\rangle(R_k+\tau_{nk}-\tau_{mk}) - \sum_{\mathbf{RP}}\frac{2}{3}\langle\mathbf{0}l|\tilde{r}_i|\mathbf{R}m\rangle\langle\mathbf{R}m|\tilde{r}_j|\mathbf{P}n\rangle\langle\mathbf{P}n|\tilde{r}_k|\mathbf{0}l\rangle\right]. \tag{30}$$

We find this form more convenient because it separates the contributions of diagonal and off-diagonal elements of position operators. (It is also manifestly invariant to the reassignment of a WF to a neighboring cell. Furthermore, note that while Eqs. (22), (27), and (30) are all equivalent as a whole, the division of contributions between the first and second terms is different in each case.) The validity of Eqs. (27) and (30) has been tested numerically by comparing with the evaluation of Eq. (22) for the case of a tight-binding model introduced in Ref. 11. The evaluated expressions agreed to numerical accuracy after extrapolation to the infinitely dense mesh. These expressions can also be shown to be gauge invariant by working directly within the Wannier representation.

C. Computational details

Calculations of the electronic ground state and of structural relaxations were performed using the QUANTUM-ESPRESSO package,[33] and the WANNIER90 code[34] was used for constructing maximally localized WFs. We used radial-grid discretized HGH (Ref. 35) norm-conserving pseudopotentials. Calculations were performed in the noncollinear spin framework. QUANTUM-ESPRESSO incorporates the spin-orbit interaction at the level of the pseudopotentials, which is a good approximation since the relativistic effects arise predominantly from the core region. The pseudopotentials used for Cr, Fe, and Gd contain semicore states in the valence, while the ones for Al, Bi, Se, and O do not. In all calculations, we used the Perdew-Wang[36] local-density approximation (LDA) energy functional.

The self-consistent calculations on Cr_2O_3were performed on a $4\times4\times4$ Monkhorst-Pack[37] grid in k space. Non-self-consistent calculations for the WF construction were performed on k-space grids containing the origin and ranging in size from $6\times6\times6$ to $12\times12\times12$. The plane-wave energy cutoff was chosen to be 150 Ry.

In the case of Bi_2Se_3, the self-consistent calculations were performed on a $6\times6\times6$ grid with energy cutoff of 60 Ry, while the non-self-consistent calculation was done on grids between $6\times6\times6$ and $11\times11\times11$.

The position-operator matrix elements $\langle\mathbf{0}m|r_j|\mathbf{R}n\rangle$ needed to evaluate Eq. (30) were calculated in k space by inverting the Fourier sum in Eq. (26) over the non-self-consistent k-point mesh and then approximating the k derivative in Eq. (19) by finite differences on that mesh, as detailed in Ref. 30.

IV. RESULTS AND DISCUSSION

A. Conventional magnetoelectrics

In this section, we present the results of our first-principles electronic-structure calculations of θ. We begin with

conventional magnetoelectrics, i.e., materials that are already experimentally known to have a nonzero magnetoelectric tensor. Some of these materials do not allow all diagonal components of the magnetoelectric tensor to be nonzero. We omit those materials from our analysis here, since we are interested in calculating the CSOMP part of the magnetoelectric coupling, which would vanish in such cases. We first present our results on Cr_2O_3 in some detail, and then briefly discuss our results for $BiFeO_3$ and $GdAlO_3$.

1. Calculation of θ in Cr_2O_3

We first fully relax the structure in the $R\bar{3}c$ space group and obtain the Wyckoff position to be $x = 0.1575$ for Cr atoms (4c orbit) and $x = -0.0690$ for O (6e orbit). The length of the rhombohedral lattice vector is $a = 5.3221$ Å while the rhombohedral angle is 53.01°. The Cr atoms have magnetic moments pointing along the rhombohedral axis as illustrated in Fig. 4(a) in an antiferromagnetic arrangement. The value of the magnetic moment is $2.0\mu_B$ per Cr atom and the electronic gap is 1.3 eV, which agrees well with previous LDA + U calculations[38,39] in the limit where the on-site Coulomb parameter U is set to zero.

Neglecting, for a moment, the magnetic spins on the Cr sites, the space-group generators are a threefold rotation, a twofold rotation, and an inversion symmetry as indicated in Fig. 4(a). Therefore, its point group is $\bar{3}m$. If we now include the spins on the Cr atoms in the analysis, we find that the threefold and twofold rotations remain, while the inversion becomes a symmetry only when combined with time reversal. Therefore, the magnetic point group of Cr_2O_3 is $\bar{3}'m'$.[40] This magnetic point group allows θ to be different from 0 or π, as discussed in Sec. II E.

Figure 5 shows the calculated values of θ using Eq. (30) for Cr_2O_3 with k-space meshes of various densities. The line indicates the second-order polynomial extrapolation to an infinitely dense mesh. The extrapolated value of θ is 1.3×10^{-3}, which is a small fraction of the quantum of OMP $\theta = 2\pi$ and corresponds to $\alpha_{xx}^{EH} = \alpha_{yy}^{EH} = \alpha_{zz}^{EH} = 0.01$ ps/m. The positive sign of θ pertains to the pattern of Cr magnetic moments shown in Fig. 4(a); reversal of all magnetic moments would flip the sign of θ.

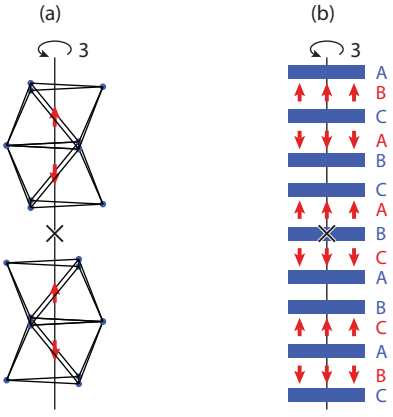

FIG. 4. (Color online) (a) Rhombohedral unit cell of Cr_2O_3. Magnetic moments on Cr atoms are indicated by red arrows, and oxygen octahedra are drawn around each Cr atom. (b) Schematic of hexagonal unit cell of Bi_2Se_3 with imposed local Zeeman field on Bi atoms. Induced magnetic moments are shown by red arrows. Thick blue lines indicate Se layers; letters (A,B,C) indicate the stacking sequence of the hexagonal layers. In both panels, the vertical line indicates the threefold rhombohedral axis, and the cross designates a twofold rotation axis orthogonal to the plane of the figure (also a center of inversion coupled with time reversal).

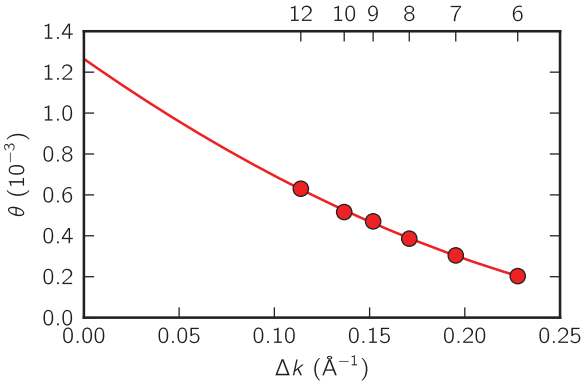

FIG. 5. (Color online) Calculated value of θ in Cr_2O_3 for varying densities of k-space grids, where Δk is the nearest-neighbor distance on the grid. The top axis specifies the size of the corresponding uniform Monkhorst-Pack grid. The line indicates a quadratic extrapolation of θ to the infinitely dense k mesh.

In order to compare this purely isotropic component of the magnetoelectric coupling with experimental values and other theoretical calculations of the full magnetoelectric response, which is not entirely isotropic, we somewhat arbitrarily define

$$\alpha^{\text{eff}} = \frac{|\alpha_{xx}| + |\alpha_{yy}| + |\alpha_{zz}|}{3}. \tag{31}$$

The value of α^{eff} obtained from the results of Ref. 8 is 0.23 ps/m for the purely electronic part of the spin-mediated component. Therefore, our calculated CSOMP contribution in Cr_2O_3 amounts to only 4% of this electronic-spin component. The ionic component of the spin response calculated by the same authors results in $\alpha^{\text{eff}} = 0.74$ ps/m, while the one calculated in Ref. 7 is about 2.6 times smaller, 0.29 ps/m. (In both of these calculations, α_{zz} is zero.) Finally, experimental measurements of the magnetoelectric tensor in Cr_2O_3 at 4.2 K vary between $\alpha^{\text{eff}} = 0.55$ and 1.17 ps/m (see Refs. 27 and 28, respectively).

Clearly, our computed CSOMP contribution for Cr_2O_3 is negligible, being 2 orders of magnitude smaller than the dominant lattice-mediated spin contribution. This is probably not surprising, since the spin-orbit coupling is relatively weak in this material. Given that it is weak, we can guess that that magnitude of the CSOMP should be linear in the strength of the spin-orbit interaction in Cr_2O_3. Our calculations allow us to check this by varying the spin-orbit interaction strength λ_{SO} between 0 (no spin orbit) and 1 (full spin-orbit interaction). As shown in Fig. 6, if we calculate θ for various intermediate values of λ_{SO}, we see that the CSOMP does indeed depend roughly linearly on λ_{SO}.

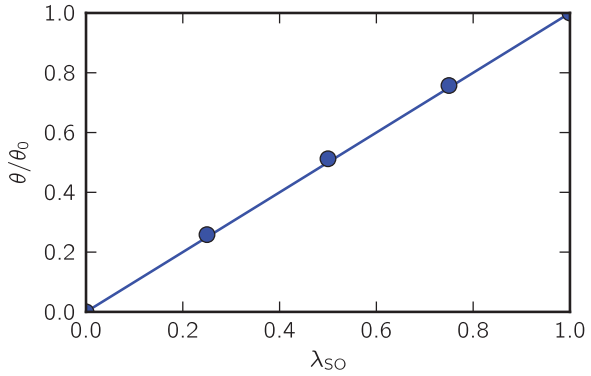

FIG. 6. (Color online) Calculated θ in Cr_2O_3 as a function of spin-orbit coupling strength, scaled such that $\lambda_{SO} = 1$ corresponds to the full spin-orbit coupling strength and $\theta_0 = \theta$ ($\lambda_{SO} = 1$).

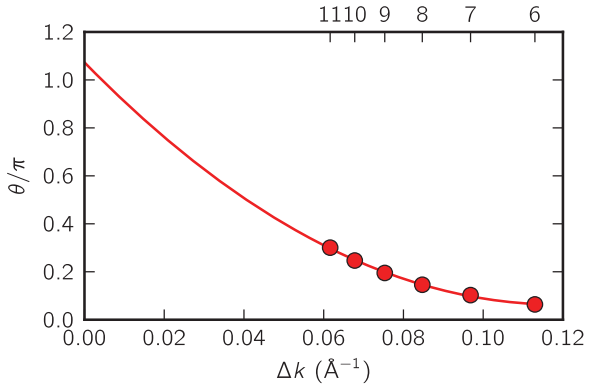

FIG. 7. (Color online) Calculated value of θ in Bi_2Se_3 for varying densities of k-space grids, where Δk is the nearest-neighbor distance on the grid. The top axis specifies the size of the corresponding uniform Monkhorst-Pack grid. The line indicates a quadratic extrapolation of θ to the infinitely dense k mesh.

2. *Other conventional magnetoelectrics*

We have also carried out calculations of θ in $BiFeO_3$ and $GdAlO_3$but with a smaller number of k-point grids than in the case of Cr_2O_3. Therefore, our results are less accurate but should still give a correct order-of-magnitude estimate of θ.

For $BiFeO_3$, we perform the calculation in the ten-atom antiferromagnetic unit cell (the long-wavelength spin spiral was suppressed). We obtain an electronic band gap of 0.95 eV with magnetic moments of $3.5\mu_B$ on each Fe atom and with a net magnetization of $0.1\mu_B$ per ten-atom primitive unit cell due to the canting of the Fe magnetic moments. Extrapolating θ to an infinitely dense mesh using just $6 \times 6 \times 6$ and $8 \times 8 \times 8$ k-point meshes, we obtain $\theta = 0.9 \times 10^{-4}$. In the case of $GdAlO_3$, we calculate the electronic band gap to be 5.0 eV and the Gd magnetic moment to be $6.7\mu_B$. We obtain a value of $\theta = 1.1 \times 10^{-4}$ after extrapolating calculations using $4 \times 4 \times 4$ and $6 \times 6 \times 6$ k-space meshes. Thus, it is clear that the CSOMP is very small in both materials.

B. Strong $\mathbb{Z}_2$ topological insulators

We now investigate the CSOMP in the case of Bi_2Se_3, which is known experimentally[17] and theoretically[41] to belong to the class of strong $\mathbb{Z}_2$ topological insulators. In the absence of broken T symmetry, such a material should have a θ of exactly $\pi \pmod{2\pi}$. We first confirm this numerically. Then, in Sec. IV C, we also study what happens when T is broken artificially by inducing antiferromagnetic order on the Bi atoms and tracking the resulting variation of θ.

Bi_2Se_3 is known to belong to space group $R\bar{3}m$, with Bi at a 2c site and Se at the high-symmetry 1a site as well as at a 2c site. In our calculations, we find that the Wyckoff parameters for Bi and Se are $x = 0.4013$ and 0.2085, respectively. We also find the length of the rhombohedral lattice vector to be $a = 9.5677$ Å and the rhombohedral angle to be only 24.77°. The electronic gap is calculated to be 0.4 eV.

The generators of the $R\bar{3}m$ space group are again threefold and twofold rotations and inversion (point group $\bar{3}m$). Since the system is nonmagnetic, the magnetic space group also contains the T-symmetry operator, and its magnetic point group is $\bar{3}m1'$. Therefore, according to the analysis given in Sec. II E, it is clear that θ must be zero or $\pi \pmod{2\pi}$.

Since we know that Bi_2Se_3 is a strong $\mathbb{Z}_2$ topological insulator, we expect that θ should be equal to $\pi \pmod{2\pi}$. However, special care needs to be taken in order to evaluate θ in such a case, because the choice of a smooth gauge becomes problematic. Specifically, it is known that the $\mathbb{Z}_2$ topology presents an obstruction to the construction of a Wannier representation (or equivalently, a smooth gauge in k space) that respects T symmetry.[42,43] Therefore, during the maximal localization procedure, one needs to choose trial WFs that do *not* take the form of Kramers pairs, thereby explicitly breaking the T symmetry.[44] (It is important to note that this choice of WFs does not bias our calculation toward having $\theta = \pi$, since the same starting choice of T-symmetry-broken WFs for a normal T-symmetric insulator would result in $\theta = 0$ up to the numerical accuracy of the calculation.)

Our results for θ in Bi_2Se_3 are given in Fig. 7 for various densities of k meshes, ranging from $6 \times 6 \times 6$ to $11 \times 11 \times 11$. A quadratic polynomial extrapolation for the infinitely dense mesh limit gives $\theta = 1.07\pi$. This is in reasonable agreement with the expected value of $\theta = \pi$, given the uncertainties in the extrapolation. (Of course, if we make a time-reversed choice of starting WFs, we obtain $\theta = -1.07\pi$, which is consistent, within the errors, with $\theta = -\pi$ and mod 2π to $\theta = \pi$.) Clearly, the convergence with respect to mesh density is somewhat slow, making a precise extrapolation difficult. The reasons for this, and some possible paths to improvement, will be discussed in Sec. V.

C. $\mathbb{Z}_2$-derived nontopological insulators with broken symmetries

Although $\theta = \pi$ in Bi_2Se_3, a finite sample with T symmetry preserved everywhere, including at the surfaces, will not exhibit any magnetoelectric coupling. From the point of view of the discussion in Sec. II D, this happens because of an exact cancellation between $\theta = \pm\pi$ contributions coming from the bulk (α) and metallic surface (Δ) terms in Eq. (16). However, if one breaks the T symmetry in the bulk (and possibly some other bulk symmetries, as detailed in Sec. II E), the CSOMP term can be allowed.

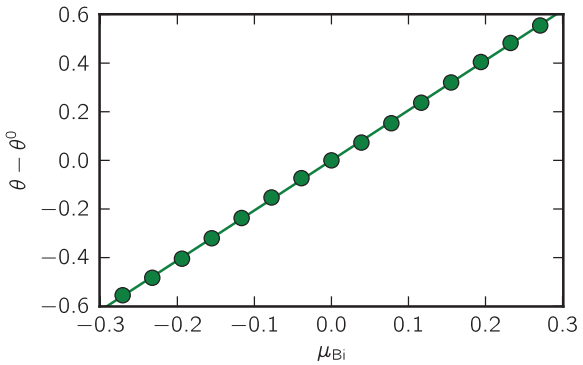

FIG. 8. (Color online) Calculated value of θ (vertical axis) and induced magnetic moment on the Bi atom (horizontal axis) for Bi_2Se_3 with artificially applied staggered Zeeman field on Bi atoms, as described in the text. θ^0 is the value of CSOMP when the magnetic field is not present.

The magnetic space group of Bi_2Se_3 contains both T and spatial-inversion symmetries. The presence of either by itself is enough to ensure that $\theta = 0$ or $\pi \pmod{2\pi}$. Now, let us consider turning on, by hand, a local Zeeman field on each Bi atom in the staggered arrangement shown in Fig. 4(b), i.e., with fields oriented parallel to the rhombohedral axis and alternating in sign. The induced magnetic moments along the threefold axis preserve both threefold and twofold rotation symmetries; both inversion and T symmetries are broken, but T taken together with inversion is still a symmetry. The resulting magnetic point group of the system is again $\bar{3}'m'$, as it was for Cr_2O_3, and it does allow for a CSOMP (the same magnetic arrangement has also been discussed in Ref. 45 in a different context).

In the density-functional calculation, one can easily apply a local Zeeman field to individual atoms in an arbitrary direction.[46] Using this method, we have calculated the CSOMP in Bi_2Se_3 with the pattern of local fields described previously and illustrated in Fig. 4(b). Figure 8 presents the calculated values of θ as a function of induced magnetic moment on Bi, where a positive μ_{Bi} corresponds to the pattern of magnetic moments indicated in Fig. 4(b). (Actually this was done by applying the full extrapolation procedure of Fig. 7 for one case, $\mu_{Bi} = 0.16\mu_B$, and using this to scale the results calculated on the $10 \times 10 \times 10$ grid at other μ_{Bi}.) The dependence of the change in CSOMP on the magnetic moment is linear over a wide range. One can see that, for a relatively moderate magnetic moment of $\pm 0.27\mu_B$, the value of θ is changed from π to $\pi \pm 0.55$. (For much higher local magnetic fields, Bi_2Se_3 becomes metallic, and the CSOMP becomes ill defined.)

These results indicate that it is possible, at least in principle, for a magnetic material to have a large but unquantized value of θ, thereby providing an incentive for future searches for materials in which such a state arises spontaneously, without the need to apply perturbations by hand as done here.

V. SUMMARY AND OUTLOOK

In this paper, we have presented a first-principles method for calculating the Chern-Simons orbital magnetoelectric coupling in the framework of density-functional theory. We have also carried out calculations of this coupling for a few well-known magnetoelectric materials, namely, Cr_2O_3, $BiFeO_3$, and $GdAlO_3$. Unfortunately, in these materials, the CSOMP contribution to the total magnetoelectric coupling is quite small. This is not surprising, since in most magnetoelectric materials, the coupling is expected to be dominated by the lattice-mediated response, whereas, the CSOMP is a purely electronic (frozen-ion) contribution. Moreover, the CSOMP is part of the orbital frozen-ion response, which is again expected to be smaller than the spin response, except perhaps in systems with very strong spin-orbit coupling, as discussed in Sec. I. For example, in Cr_2O_3, the CSOMP is about 4% of the frozen-ion spin contribution to the magnetoelectric coupling.

On the other hand, we have reason to believe that, in special cases, the CSOMP contribution to the magnetoelectric coupling could be large compared to the total magnetoelectric coupling in known magnetoelectrics, such as Cr_2O_3. After all, as already pointed out in Sec. II D 2, $\mathbb{Z}_2$ topological insulators are predicted to display a large magnetoelectric effect of purely orbital origin when their surfaces are gapped in an appropriate way. If this is so, why should a similar effect not occur in certain T-broken systems?

As a proof of concept for the existence of those special cases, we have considered Bi_2Se_3 with inversion and time-reversal symmetries explicitly broken by hand. Here, we find that, with a relatively modest induced magnetic moment on the Bi atoms, one can still achieve quite a large change in the CSOMP.

On the computational side, several challenges still remain. For example, the convergence of our calculations of the CSOMP with respect to the k-point mesh density is disappointingly slow. A direct calculation of θ in Bi_2Se_3 using a very dense mesh of $11 \times 11 \times 11$ k points only manages to recover about 30% of the converged value of $\theta = \pi$, and an extrapolation procedure is needed to bring us within 10% of that value. This clearly points to the need for methodological improvements, and we now comment briefly on some possible paths for future work.

The slow convergence that we observe is related, in part, to the way in which we evaluate the position-operator matrix elements $\langle \mathbf{0}m|r_j|\mathbf{R}n\rangle$. As discussed in Ref. 30, the k-space procedure we adopted (see Sec. III C) entails an error of $O(\Delta k^2)$. Preliminary tests on a tight-binding model suggest that an exponentially fast convergence of θ can be achieved by an alternative procedure, in which the WFs are first constructed on a real-space grid over a supercell (whose size scales with the k-mesh density), and the position matrix elements are then evaluated directly on that grid, as in Ref. 47. It may also be possible to improve the k-space calculation by using higher-order finite-difference formulas that have a more rapid convergence with respect to mesh density.

An alternative approach would be to develop a formula for the CSOMP that is exactly gauge invariant in the case of a discretized k-space grid. Such an expression already exists for the case of electronic polarization, Eq. (23), but we are aware of no counterpart for the CSOMP. Although such an approach would not necessarily provide much faster convergence with respect to the k-space sampling, it would still be a significant improvement. For example, one would not need to construct a smooth gauge in k space, which is a particular problem in the case of $\mathbb{Z}_2$ insulators (or for a symmetry-broken insulator in the

vicinity of a $\mathbb{Z}_2$ phase). Another use of such a formula would be to calculate the $\mathbb{Z}_2$ index of any insulator with relative ease, even in the cases when other methods[48–50] cannot be applied (for example, when inversion symmetry is not present).

Furthermore, a full calculation of the electronic contribution to the orbital magnetoelectric response should also include the remaining two contributions given in Eqs. (6) and (7). This calculation would also require knowledge of the first derivatives of the electronic wave functions with respect to electric field. While these derivatives are available as part of the linear-response capabilities of the QUANTUM-ESPRESSO package,[33] some care is needed to arrive at a robust implementation of Eqs. (6) and (7), as will be reported in a future communication.

Finally, recall that our calculations have all been carried out in the context of ordinary density-functional theory. In cases where orbital currents play a role, it is possible that current-density functionals[51,52] could give an improved description. However, such functionals are still in an early stage of development and testing, and we prefer to focus first on exploring the extent to which conventional density functionals can reproduce experimental properties of systems in which orbital currents are present.

Overall, significant progress has been made in the ability to calculate the magnetoelectric coupling of real materials in the context of density-functional theory. The methods described in Refs. 7 and 8 allow for the calculation of both the electronic and lattice components of the spin (i.e., Zeeman) contribution to the magnetoelectric coupling. In principle, at least, the lattice component of the orbital contribution could be computed using the methods of Ref. 53, while the remaining orbital electronic contributions can be computed from the formulas derived in Refs. 10 and 11 following the developments discussed here. While we have not focused here on the contributions of Eqs. (5) and (6), we plan to present calculations of these terms in a forthcoming publication. Thus, we expect that the computation of all of the various contributions to the magnetoelectric coupling will soon be accessible to modern density-functional methods.

ACKNOWLEDGMENTS

We would like to acknowledge useful discussions with J. R. Yates and Y. Mokrousov. The work was supported by NSF Grants No. DMR-0549198, No. DMR-0706493, and No. DMR-1005838.

*sinisa@physics.rutgers.edu

[1] M. Fiebig, J. Phys. D: Appl. Phys. **38**, R123 (2005).
[2] W. Eerenstein, N. D. Mathur, and J. F. Scott, Nature (London) **442**, 759 (2006).
[3] M. Fiebig and N. A. Spaldin, Eur. Phys. J. B **71**, 293 (2009).
[4] J.-P. Rivera, Eur. Phys. J. B **71**, 299 (2009).
[5] V. E. Wood and A. E. Austin, in *Magnetoelectric Interaction Phenomena in Crystals*, edited by A. J. Freeman and H. Schmid (Gordon and Breach, London, 1975), pp. 181–194.
[6] G. A. Smolenski and I. E. Chupis, Sov. Phys. Usp. **25**, 475 (1982).
[7] J. Íñiguez, Phys. Rev. Lett. **101**, 117201 (2008).
[8] K. T. Delaney, E. Bousquet, and N. A. Spaldin, e-print arXiv:0912.1335 (to be published).
[9] J. C. Wojdel and J. Íñiguez, Phys. Rev. Lett. **103**, 267205 (2009).
[10] A. M. Essin, A. M. Turner, J. E. Moore, and D. Vanderbilt, Phys. Rev. B **81**, 205104 (2010).
[11] A. Malashevich, I. Souza, S. Coh, and D. Vanderbilt, New J. Phys. **12**, 053032 (2010).
[12] X. L. Qi, T. L. Hughes, and S.-C. Zhang, Phys. Rev. B **78**, 195424 (2008).
[13] A. M. Essin, J. E. Moore, and D. Vanderbilt, Phys. Rev. Lett. **102**, 146805 (2009).
[14] L. Fu and C. L. Kane, Phys. Rev. B **76**, 045302 (2007).
[15] D. Hsieh, D. Qian, L. Wray, Y. Xia, Y. S. Hor, R. J. Cava, and M. Z. Hasan, Nature (London) **452**, 970 (2008).
[16] D. Hsieh, Y. Xia, D. Qian, L. Wray, F. Meier, J. H. Dil, J. Osterwalder, L. Patthey, A. V. Fedorov, H. Lin, A. Bansil, D. Grauer, Y. S. Hor, R. J. Cava, and M. Z. Hasan, Phys. Rev. Lett. **103**, 146401 (2009).
[17] Y. Xia, D. Qian, D. Hsieh, L. Wray, A. Pal, H. Lin, A. Bansil, D. Grauer, Y. S. Hor, R. J. Cava, and M. Z. Hasan, Nat. Phys. **5**, 398 (2008).
[18] F. W. Hehl, Y. N. Obukhov, J.-P. Rivera, and H. Schmid, Eur. Phys. J. B **71**, 321 (2009).
[19] J.-P. Rivera, Ferroelectrics **161**, 165 (1994).
[20] R. D. King-Smith and D. Vanderbilt, Phys. Rev. B **47**, 1651 (1993).
[21] D. Vanderbilt and R. D. King-Smith, Phys. Rev. B **48**, 4442 (1993).
[22] S. Coh and D. Vanderbilt, Phys. Rev. Lett. **102**, 107603 (2009).
[23] Here, we refer to a multiband gauge transformation having the form of Eq. (18), since $\boldsymbol{\alpha}$ can be shown to be fully invariant under a single-band phase twist.
[24] F. D. M. Haldane, Phys. Rev. Lett. **93**, 206602 (2004).
[25] F. D. M. Haldane, Phys. Rev. Lett. **61**, 2015 (1988).
[26] M. Z. Hasan and C. L. Kane, Rev. Mod. Phys. **82**, 3045 (2010).
[27] H. Wiegelmann, A. G. M. Jansen, P. Wyder, J. P. Rivera, and H. Schmid, Ferroelectrics **162**, 141 (1994).
[28] E. Kita, K. Siratori, and A. Tasaki, J. Appl. Phys. **50**, 7748 (1979).
[29] A. P. Cracknell, *Magnetism in Crystalline Materials* (Pergamon, Oxford, 1975).
[30] X. Wang, J. R. Yates, I. Souza, and D. Vanderbilt, Phys. Rev. B **74**, 195118 (2006).
[31] X. Wang, D. Vanderbilt, J. R. Yates, and I. Souza, Phys. Rev. B **76**, 195109 (2007).
[32] N. Marzari and D. Vanderbilt, Phys. Rev. B **56**, 12847 (1997).
[33] P. Giannozzi, S. Baroni, N. Bonini, M. Calandra, R. Car, C. Cavazzoni, D. Ceresoli, G. L. Chiarotti, M. Cococcioni, I. Dabo, A. Dal Corso, S. de Gironcoli, S. Fabris, G. Fratesi,

R. Gebauer, U. Gerstmann, C. Gougoussis, A. Kokalj, M. Lazzeri, L. Martin-Samos, N. Marzari, F. Mauri, R. Mazzarello, S. Paolini, A. Pasquarello, L. Paulatto, C. Sbraccia, S. Scandolo, G. Sclauzero, A. P. Seitsonen, A. Smogunov, P. Umari, and R. M. Wentzcovitch, J. Phys. Condens. Matter **21**, 395502 (2009).

[34]A. A. Mostofi, J. R. Yates, Y.-S. Lee, I. Souza, D. Vanderbilt, and N. Marzari, Comput. Phys. Commun. **178**, 685 (2008).

[35]C. Hartwigsen, S. Goedecker, and J. Hutter, Phys. Rev. B **58**, 3641 (1998).

[36]J. P. Perdew and Y. Wang, Phys. Rev. B **45**, 13244 (1992).

[37]H. J. Monkhorst and J. D. Pack, Phys. Rev. B **13**, 5188 (1976).

[38]N. J. Mosey and E. A. Carter, Phys. Rev. B **76**, 155123 (2007).

[39]S. Shi, A. L. Wysocki, and K. D. Belashchenko, Phys. Rev. B **79**, 104404 (2009).

[40]Throughout the paper, the notation for magnetic point groups follows Ref. 29.

[41]H. Zhang, C.-X. Liu, X.-L. Qi, X. Dai, Z. Fang, and S.-C. Zhang, Nat. Phys. **5**, 438 (2008).

[42]L. Fu and C. L. Kane, Phys. Rev. B **74**, 195312 (2006).

[43]R. Roy, Phys. Rev. B **79**, 195321 (2009).

[44]A. A. Soluyanov and D. Vanderbilt, Phys. Rev. B **83**, 035108 (2011).

[45]R. Li, J. Wang, X.-L. Qi, and S.-C. Zhang, Nat. Phys. **6**, 284 (2010).

[46]This is done by adding an energy penalty term of the form $\lambda \sum_i (\boldsymbol{\mu}_i - \bar{\boldsymbol{\mu}}_i)^2$ to the Kohn-Sham energy functional, where $\boldsymbol{\mu}_i$ is the actual value of the magnetic moment of the ith atom in the unit cell while $\bar{\boldsymbol{\mu}}_i$ and λ are adjustable parameters. The moments $\boldsymbol{\mu}_i$ are calculated by integrating the spin density within atom-centered spheres.

[47]M. Stengel and N. A. Spaldin, Phys. Rev. B **73**, 075121 (2006).

[48]L. Fu, C. L. Kane, and E. J. Mele, Phys. Rev. Lett. **98**, 106803 (2007).

[49]J. E. Moore and L. Balents, Phys. Rev. B **75**, 121306 (2007).

[50]R. Roy, Phys. Rev. B **79**, 195322 (2009).

[51]G. Vignale and M. Rasolt, Phys. Rev. B **37**, 10685 (1988).

[52]G. Vignale, Phys. Rev. B **70**, 201102 (2004).

[53]D. Ceresoli, T. Thonhauser, D. Vanderbilt, and R. Resta, Phys. Rev. B **74**, 024408 (2006).